

## Potent and selective CK2 kinase inhibitors with effects on Wnt pathway signaling in vivo

James E Dowling, Marat Alimzhanov, Larry Bao, Claudio Chuaqui, Christopher Denz, Emma L Jenkins, Nicholas Larsen, Paul D Lyne, Timothy Pontz, Qing Ye, Geoffrey Allan Holdgate, Lindsay Snow, Nichole O'Connell, and Andrew D. Ferguson

ACS Med. Chem. Lett., **Just Accepted Manuscript** • DOI: 10.1021/acsmchemlett.5b00452 • Publication Date (Web): 20 Jan 2016

Downloaded from <http://pubs.acs.org> on January 25, 2016

### Just Accepted

"Just Accepted" manuscripts have been peer-reviewed and accepted for publication. They are posted online prior to technical editing, formatting for publication and author proofing. The American Chemical Society provides "Just Accepted" as a free service to the research community to expedite the dissemination of scientific material as soon as possible after acceptance. "Just Accepted" manuscripts appear in full in PDF format accompanied by an HTML abstract. "Just Accepted" manuscripts have been fully peer reviewed, but should not be considered the official version of record. They are accessible to all readers and citable by the Digital Object Identifier (DOI®). "Just Accepted" is an optional service offered to authors. Therefore, the "Just Accepted" Web site may not include all articles that will be published in the journal. After a manuscript is technically edited and formatted, it will be removed from the "Just Accepted" Web site and published as an ASAP article. Note that technical editing may introduce minor changes to the manuscript text and/or graphics which could affect content, and all legal disclaimers and ethical guidelines that apply to the journal pertain. ACS cannot be held responsible for errors or consequences arising from the use of information contained in these "Just Accepted" manuscripts.

# Potent and selective CK2 kinase inhibitors with effects on Wnt pathway signaling *in vivo*

James E. Dowling<sup>a\*</sup>, Marat Alimzhanov<sup>a</sup>, Larry Bao<sup>a</sup>, Claudio Chuaqui<sup>a</sup>, Christopher R. Denz<sup>a</sup>, Emma Jenkins<sup>a</sup>, Nicholas A. Larsen<sup>a</sup>, Paul D. Lyne<sup>a</sup>, Timothy Pontz<sup>a</sup>, Qing Ye<sup>a</sup>, Geoff A. Holdgate<sup>b</sup>, Lindsay Snow<sup>b</sup>, Nichole O'Connell<sup>c</sup> and Andrew D. Ferguson<sup>c</sup>

<sup>a</sup> AstraZeneca R&D, Oncology Innovative Medicines Unit, 35 Gatehouse Drive, Waltham, MA 02451, USA

<sup>b</sup> AstraZeneca R&D, Structure & Biophysics, Discovery Sciences, Darwin Building, 310 Cambridge Science Park, Milton Road, Cambridge, CB4 0WG UK

<sup>c</sup> AstraZeneca R&D, Structure & Biophysics, Discovery Sciences 35 Gatehouse Drive, Waltham, MA 02451 USA

**KEYWORDS:** CK2 kinase, pyrazolo[1,5-*a*]pyrimidine, Wnt,  $\beta$ -catenin

**ABSTRACT:** The Wnt pathway is an evolutionarily conserved and tightly regulated signaling network with important roles in embryonic development and adult tissue regeneration. Impaired Wnt pathway regulation, arising from mutations in Wnt signaling components, such as Axin, APC and  $\beta$ -catenin, results in uncontrolled cell growth and triggers oncogenesis. To explore the reported link between CK2 kinase activity and Wnt pathway signaling, we sought to identify a potent, selective inhibitor of CK2 suitable for proof of concept studies *in vivo*. Starting from a pyrazolo[1,5-*a*]pyrimidine lead (**2**), we identified compound **7h**, a potent CK2 inhibitor with picomolar affinity that is highly selective against other kinase family enzymes and inhibits Wnt pathway signaling ( $IC_{50} = 50$  nM) in DLD-1 cells. In addition, compound **7h** has physicochemical properties that are suitable for formulation as an intravenous solution, has demonstrated good pharmacokinetics in preclinical species, and exhibits a high level of activity as a monotherapy in HCT-116 and SW-620 xenografts

The serine/threonine protein kinase CK2 is a constitutively active heterotetrameric complex composed of two catalytic ( $\alpha$  or  $\alpha'$ ) and two regulatory ( $\beta$ ) subunits,<sup>1</sup> which has emerged as an attractive drug discovery target in oncology.<sup>2</sup> Researchers from Cylene have recently advanced CX-4945, a selective, orally available inhibitor of CK2 into the clinic for treatment of patients with solid tumors and haematological malignancies.<sup>3</sup>

Among its diverse functions, CK2 interacts with and regulates multiple components of the Wnt pathway, an evolutionarily-conserved signaling network that regulates embryonic development and the regeneration of intestinal epithelial cells.<sup>4</sup> Certain cancers, including colorectal carcinoma (CRC), arise due to gene mutations among constituents of the Wnt pathway, including the CK2 substrates dishevelled (Dvl), APC and  $\beta$ -catenin.<sup>5</sup> Inhibition of CK2, either by RNA knockdown or with small molecules, decreases  $\beta$ -catenin-Tcf-mediated transcriptional of Wnt target genes such as survivin and leads to cell death and apoptosis in a range of CRC lines.<sup>6,7</sup> In addition, elevated levels of CK2 activity have been reported in CRC tissue samples and expression levels correlate with poor prognosis in CRC patients.<sup>8,9</sup> Taken together, these data illustrate the potential utility of CK2 inhibitors in CRC and other cancers characterized by aberrant Wnt pathway activity.

We sought to identify a potent, selective inhibitor of CK2 kinase for hypothesis testing *in vivo* using preclinical models of CRC. An early probe from our previously-described series of ATP-competitive pyrazolo[1,5-*a*]pyrimidine-derived inhibitors of CK2 (**1**, **2**; Figure 1) was used to assess the link between CK2 inhibition and Wnt signaling.<sup>10</sup>

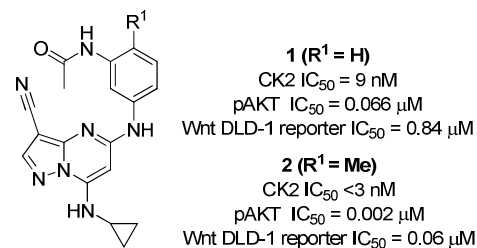


**Figure 1.** Early pyrazolo[1,5-*a*]pyrimidine leads (**1** & **2**).

Treatment of DLD-1(APC mutant) cells with **2** inhibits  $\beta$ -catenin phosphorylation and decreases Wnt-mediated gene transcription as shown in a Luciferase reporter assay in APC mutant DLD-1 cells ( $IC_{50} = 0.06$   $\mu$ M).<sup>11</sup> In an acute dose pharmacokinetic/pharmacodynamic (PK/PD) study, treatment of DLD-1/AKT1 over-expressing murine xenografts with **2** (10 mg/kg, PO) resulted in the 20% inhibition of Wnt-mediated luciferase gene transcription at 8 hours, and coincided with an unbound drug concentration at the level of the Wnt reporter  $IC_{50}$ . When tested in disease model studies using a murine DLD-1(APC<sup>mut</sup>) xenograft, compound **2** showed limited tumor growth inhibition.<sup>10</sup>

Our medicinal chemistry strategy subsequently focused on achieving potent inhibition of the Wnt pathway, as demonstrated using a Wnt luciferase reporter assay in DLD-1 cells,<sup>11</sup> while seeking to improve physicochemical properties, enhance target coverage, and potentially deliver increased *in vivo* efficacy in preclinical models characterized by aberrant Wnt signaling.

To aid our design efforts we obtained the X-ray crystallographic structure of human CK2 $\alpha$  at 2.55 Å resolution in complex with compound **2**.<sup>12</sup> The inhibitor occupies the ATP-binding cleft and is anchored to the hinge region via a pair of hydrogen bonds. The C7 aminocyclopropane group is directed toward solvent and forms a hydrogen bond with the main-chain carbonyl oxygen of V116 while the N1 position of the pyrazolopyrimidine core interacts with the amide NH of the same residue. An additional interaction is observed between an ordered water molecule and the C5 NH of the inhibitor. The *ortho*-methyl substituent enforces an energetically disfavored *cisoid* configuration of the acetamide that permits coordination of the carbonyl group with a nearby water molecule. This bound water, adjacent to the gatekeeper residue F113, also interacts with the cyano group of the pyrazolo[1,5-*a*]pyrimidine core and the main-chain amide of D175. In addition, the solved structure suggested that substitution of the *ortho*- position (R<sup>1</sup> in Figure 1, Scheme 1 and Table 1) with polar functionality could enable additional energetically favorable interactions with the protein.

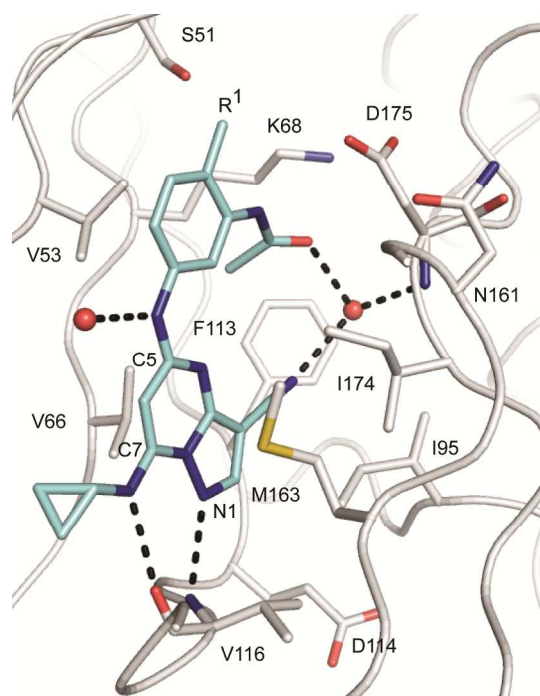
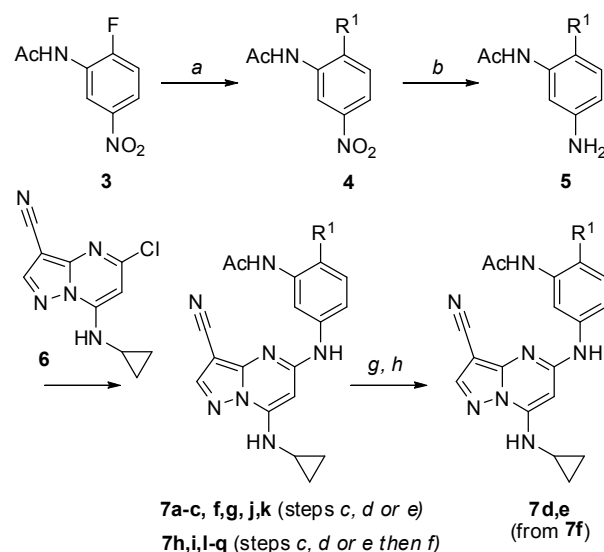


**Figure 2.** X-ray crystallographic structure of human CK2 $\alpha$  in complex with compound **2** determined at 2.55 Å resolution (PDB accession code: 5H8B).<sup>12, 13</sup> Water molecules are shown as red spheres. Hydrogen bonds to the inhibitor are shown as black dashed lines.<sup>14</sup>

Analogues of **2** were synthesized by adapting the convergent approach described in our earlier work (Scheme 1).<sup>10</sup> Treatment of *N*-(2-fluoro-5-nitro-phenyl)acetamide (**3**) with secondary amines, followed by reduction of the nitro group in the resulting products (**4**), afforded anilines of general structure **5**. Palladium-catalyzed or KF-promoted coupling of these intermediates (**5**) with 5-chloro-7-(cyclopropylamino) pyrazolo[1,5-*a*]pyrimidine-3-carbonitrile (**6**) provided the desired analogs (Table 1) either directly (**7a-c**, **f**, **g**, **j**, **k**), via the methanesulfonyl derivative of **7f** or, as in the case of **7h-i**, **l** and **q**, following TFA deprotection of the corresponding Boc derivatives (Scheme 1)

### Scheme 1<sup>a</sup> Synthesis of compounds 7a-q.

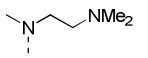
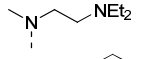
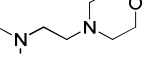
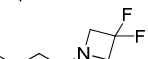
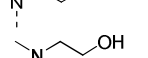
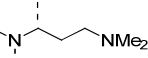
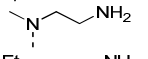
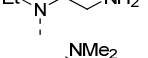
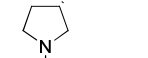
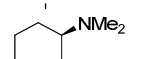
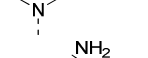
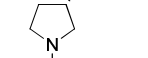
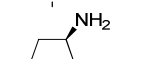
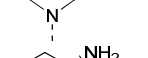
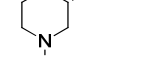
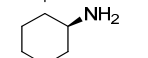


<sup>a</sup>Reagents and conditions: (a) R,R'NH, Cs<sub>2</sub>CO<sub>3</sub>, DMF, 80 °C; (b) H<sub>2</sub>, Pd/C, MeOH, 25 °C; (c) **6**, 5 mol% Xantphos, 10 mol% Pd<sub>2</sub>(dba)<sub>3</sub>, Cs<sub>2</sub>CO<sub>3</sub>, DMA, 150 °C in a microwave; (d) **6**, KF, NMP or DMSO, 150 °C; (e) **6**, 20 mol% tBuXphos, 10 mol% Pd<sub>2</sub>(dba)<sub>3</sub>, Cs<sub>2</sub>CO<sub>3</sub>, NMP/Dioxane, 100 °C; (f) TFA, CH<sub>2</sub>Cl<sub>2</sub>, 25 °C; (g) **7f**, pyridine, MsCl, 0 °C; (h) R,R'NH, MeCN, 65 °C.

Introduction of an *N*-methylpiperazinyl substituent (**7a**) enhanced solubility, but reduced enzymatic and cellular potency relative to **2**. However, the acyclic 1,2-diaminoethyl substituent of **7b** imparted high solubility in addition to potent enzymatic (CK2 IC<sub>50</sub> <3 nM) and cellular activity (Wnt DLD-1 Luciferase IC<sub>50</sub> = 75 nM). Further substitution of the terminal amino group, as in *N,N*-diethyl analogue **7c**, reduced the biochemical and cellular potency. Weakly basic or non-basic groups at the terminal position (**7d-7f**) contributed to a reduction in Wnt reporter activity. Extension of the linker segment in **7b** by an additional methylene unit, producing analogue **7g**, results in a greater than 10-fold reduction in enzyme activity and suggested that optimal positioning of the charged dimethylamino group was achieved with a three atom linker. Pharmacokinetics for **7b** in the rat following oral administration of 10 mg/kg dose are characterized by low exposure (AUC = 0.36 μM·h) and high clearance (CL = 65 mL/min/kg). *In vitro* metabolite identification studies using rat hepatocytes identified a series of products derived from **7b** that likely arise via oxidative demethylation of the side chain nitrogen atoms. Incubations in the presence of ABT in rat and human microsomes give less extensive metabolite formation and suggest a predominantly oxidative mechanism of clearance for **7b**. We subsequently synthesized the di-demethylated analogue **7h**, which exhibits improved cellular activity (Wnt DLD-1 Luciferase IC<sub>50</sub> = 50 nM), high solubility and reduced intrinsic clearance in rat hepatocytes and human microsomes relative to **7b**. In addition, **7h** showed greatly reduced activity (IC<sub>50</sub> >100 μM) compared to **7b** (IC<sub>50</sub> = 4 μM) in our hERG ion channel assay. Interestingly, rigidification of the linker segment through the use of 3-aminopyrrolidino- (**7l**, **m**) and 3-aminopiperidino- substituents (**7n**, **o**), despite contributing to an overall increase in lipophilicity, afforded compounds with reduced turnover in rat hepatocyte and human microsome preparations but led to a reduction in Wnt reporter assay po-

tency (Table 1). Substitution adjacent to the primary amine, as in **7p** and **7q**, led to further improvement in the *in vitro* metabolic stability while preserving cellular activity.

**Table 1.** Optimization of the *ortho*-substituent improves cellular potency, solubility and metabolic stability.

Cmpd	R <sup>1</sup>	CK2 $\alpha$	pAKT <sup>S129</sup>	Wnt DLD-1	Sol.	Hu PPB	Hu Mics CL <sub>int</sub> <sup>b</sup>	Rat Heps CL <sub>int</sub> <sup>b</sup>
		IC <sub>50</sub> ( $\mu$ M) <sup>a</sup>	IC <sub>50</sub> ( $\mu$ M) <sup>a</sup>	IC <sub>50</sub> ( $\mu$ M) <sup>a</sup>	pH 7.4 ( $\mu$ M)	(% free)	( $\mu$ L/min/mg)	( $\mu$ L/min/10 <sup>6</sup> )
<b>1</b>	H	0.009	0.066	0.60	15	5	20	26
<b>2</b>	Me	<0.003	0.002	0.060	8	10	10	5
<b>7a</b>	4-methylpiperazin-1-yl	0.041	0.27	1.1	570	18	<4	7
<b>7b</b>		<0.003	0.001	0.075	>1000	26	9	32
<b>7c</b>		0.009	0.019	0.39	>1000	23	44	27
<b>7d</b>		<0.003	0.005	0.30	275	18	135	>300
<b>7e</b>		0.013	0.14	0.76	241	2	ND	ND
<b>7f</b>		<0.003	ND	0.32	2	7	21	17
<b>7g</b>		0.006	ND	0.73	>1000	22	<4	15
<b>7h</b>		<0.003	0.004	0.043	>1000	39	7	8
<b>7i</b>		<0.003	ND	0.032	>1000	30	5	2
<b>7j</b>		0.006	0.016	0.38	>800	29	9	2.5
<b>7k</b>		0.004	0.031	0.51	>900	11	19	<1
<b>7l</b>		<0.003	0.07	0.69	590	31	<3	<1
<b>7m</b>		<0.003	0.07	0.96	812	32	<3	2.5
<b>7n</b>		<0.003	0.008	0.18	704	22	<3	<1
<b>7o</b>		0.005	0.08	0.65	>1000	20	<3	<1
<b>7p</b>		<0.003	0.004	0.40	825	33	<3	<1
<b>7q</b>		<0.003	0.004	0.67	895	36	<3	<1

<sup>a</sup>Mean value of two experiments. Deviations were within  $\pm 25\%$ ; <sup>b</sup>Intrinsic clearance (CL<sub>int</sub>) determined from human liver microsome incubations ( $\mu$ L/min/mg) or rat hepatocyte incubations ( $\mu$ L/min/10<sup>6</sup> cells); ND = not determined

To confirm our initial design hypothesis, we determined the X-ray crystallographic structures of CK2 $\alpha$  with **7b** and **7h** (Figure 3).<sup>12</sup> Both inhibitors are bound in the ATP-binding site in a manner analogous to that of **2**. However, while the sidechain of **7b** positions the terminal dimethylamino group for an electrostatic interaction with D175, the unsubstituted amine of **7h** is able to directly coordinate an ordered water molecule and the side-chain carbonyl group of N161.

A number of compounds in this series possess half-maximum inhibitory potency below the lower limit of detection (IC<sub>50</sub> < 3 nM) in our enzymatic assay, which measures the inhibition of recombinant human full-length CK2 $\alpha$  mediated phosphorylation of a synthetic peptide substrate at K<sub>m</sub> ATP concentration. To better understand the contribution of the side-chain interactions on ligand binding we developed a Surface Plasmon Resonance (SPR) assay to determine the binding affinities of **2**, **7b** and **7h**.<sup>14</sup> The results, (Table 2) indicate that

1  
2  
3  
4  
5  
6  
7  
8  
9  
10  
11  
12  
13  
14  
15  
16  
17  
18  
19  
20  
21  
22  
23  
24  
25  
26  
27  
28  
29  
30  
31  
32  
33  
34  
35  
36  
37  
38  
39  
40  
41  
42  
43  
44  
45  
46  
47  
48  
49  
50  
51  
52  
53  
54  
55  
56  
57  
58  
59  
60

**2** and **7h** possess similar affinity and are approximately 10-fold more potent than **7b**. Comparison of **7b** and **7h** indicate that the dimethylamino side-chain of **7b** is disfavored compared to the primary amine of **7h**.

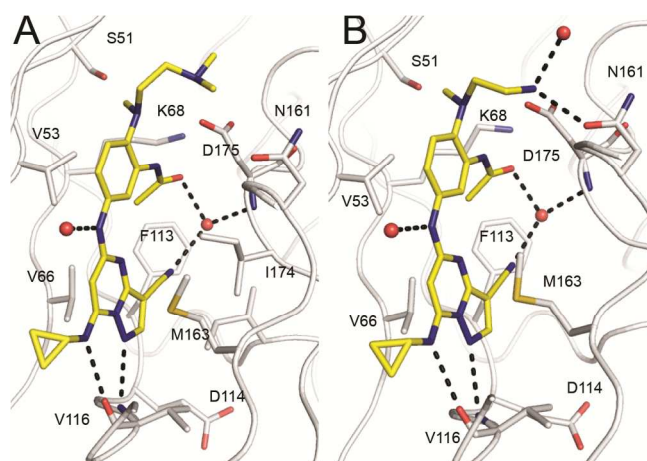


**Figure 3.** X-ray crystallographic structure of human CK2 $\alpha$  in complex with compounds **7b** (A) and **7h** (B) determined at 2.00 Å and 2.15 Å resolution (PDB accession codes: 5H8G and 5H8E).<sup>12,13</sup> Water molecules are shown as red spheres and hydrogen bonds to the inhibitor are shown as black dashed lines.

**Table 2.** CK2 $\alpha$  SPR Data.

Compound	K <sub>D</sub> (pM)
<b>2</b>	4.91 ± 1.64
<b>7b</b>	48.2 ± 5.78
<b>7h</b>	6.33 ± 0.054

Kinase selectivity profiling of **7h** at a concentration of 0.1 μM against a panel of 402 kinases revealed a high degree of selectivity (Figure 4).<sup>15</sup> The limited off-target activity (12 kinases with > 50 % inhibition) was restricted to members of the CMGC family, including isoforms of the dual-specificity tyrosine-regulated kinases (Dyrk) and CAMK kinases such as the death-associated protein kinases (Dapk) and homeodomain interacting protein kinases (Hipk). Moderate inhibition (74%) of bone morphogenetic protein receptor type-1B kinase (BMPR1b) was also observed. Biochemical IC<sub>50</sub> determinations ([ATP] = K<sub>m</sub>) revealed that **7h** exhibits moderate-to-weak activity against the Hipk and Dyrk isoforms (IC<sub>50</sub>s = 0.04 - 1.3 μM), and is active in the 10-20 nM range against Dapk2 and Dapk3.<sup>14</sup>

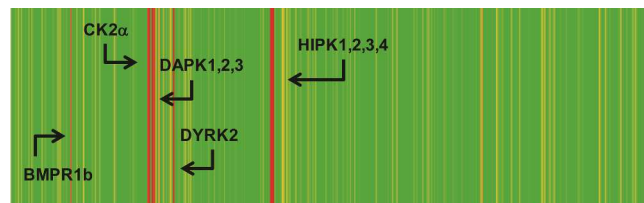


**Figure 4.** Kinase selectivity profile for **7h** when tested at a concentration of 0.1 μM against a panel of 402 kinases.

The ability of our compounds to inhibit the Wnt pathway, as measured using the DLD-1 Topflash reporter assay, correlates well with inhibition of a direct CK2 substrate, pAKT<sup>S129</sup>, in cells.<sup>16</sup> These data are consistent with the finding that CK2 $\alpha$ -dependent up-regulation of  $\beta$ -catenin driven transcriptional activity requires phosphorylation of AKT.<sup>17</sup> In addition, Wnt pathway inhibition correlates with antiproliferative effects in DLD-1 (APC mutant) cells (Figure 5). Similar levels of activity are observed in other CRC cell lines with constitutively activated Wnt signaling that is driven either by  $\beta$ -catenin (HCT-116) or APC mutations (SW620) (Table 3).

**Table 3.** Selected growth inhibition data.

Cpd	HCT-116	DLD-1	SW620
	GI <sub>50</sub> (μM) <sup>a</sup>	GI <sub>50</sub> (μM) <sup>a</sup>	GI <sub>50</sub> (μM) <sup>a</sup>
<b>1</b>	0.7	ND	0.7
<b>2</b>	0.08	0.17	0.1
<b>7b</b>	0.03	0.08	0.03
<b>7h</b>	0.01	0.05	0.005

<sup>a</sup>Mean value of at least three experiments; ND = not determined.

To further strengthen the mechanistic data, we subsequently demonstrated that **7h** induced a concentration-dependent decrease in the active form of  $\beta$ -catenin in Wnt3a expressing mouse fibroblast L-cells,<sup>14</sup> an *in vitro* system in which pathway up-regulation is triggered by constitutive Wnt3a expression (Figure S1). In addition, the mouse L S/L line contains a TCF4 driven luciferase construct and the degree of active  $\beta$ -catenin inhibition seen with **7h** correlates with the potency of the compound in the corresponding Wnt3a L S/L reporter assay (IC<sub>50</sub> = 0.05 μM).<sup>14</sup>

Based on the *in vitro* biomarker, pathway and growth inhibition data of **7h**, characterization of this compound *in vivo* was undertaken. Oral dosing of **7h** resulted in low bioavailability and limited the unbound drug concentration to levels expected to be sub-therapeutic. However, intraperitoneal (IP) or intravenous (IV) dosing regimens delivered sustained free drug concentrations above efficacious levels.

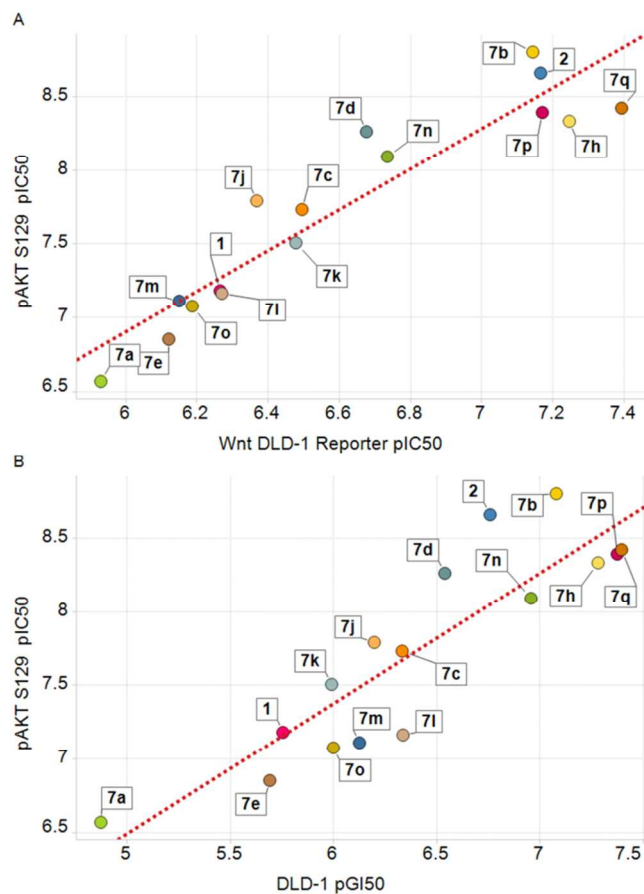


**Figure 5.** Relationship between pAKT<sup>S129</sup> depletion and Wnt Topflash reporter inhibition in DLD-1 cells (A). Relationship between pAKT<sup>S129</sup> depletion and growth inhibition in DLD-1 cells (B).

The ability of compound **7h** to inhibit substrate and downstream marker phosphorylation in an APC mutant CRC model was evaluated in SW620 tumor-bearing murine xenografts. Administration of **7h** induced dose-dependent modulation of the downstream markers pAKT<sup>S129</sup> and  $\beta$ -catenin, as determined by Western blot analysis of tumor cell lysates (Figure 6A).<sup>14</sup> Similarly, DLD-1 TOPflash luciferase (APC mutant) xenografts were utilized to assess the effect of the compound on Wnt-associated gene transcription. In this model, treatment with a single dose (10 mg/kg, IV) of **7h** led to 40-50% inhibition of Tcf4-luciferase signal at the 8h timepoint with suppression of this signal, and AKT<sup>S129</sup> phosphorylation (not shown), still evident at 24 hours, by which time no detectable drug remained in plasma (Figure 6B).

The durable substrate and pathway suppression observed with **7h** following its clearance from plasma may be due, in part, to the high (pM) affinity of the compound (Table 2) and its associated slow dissociation rate ( $k_d = 0.00025 \text{ s}^{-1}$ ). These and other data,<sup>18</sup> suggested the potential for an intermittent dosing schedule as a means to achieve activity in disease model studies while minimizing tolerability issues.

Compound **7h** showed a dose-dependent tumor growth inhibition, achieving 94% TGI in a HCT-116 ( $\beta$ -catenin mu-

tant/ model and 74% TGI in a SW620 (APC mutant) model at a 30 mg/kg dose given weekly for 3 cycles. Reversible dose-proportional body weight loss was observed in both experiments; in the SW620 study, mean body weight changes observed on day 25 in treated animals ranged from -0.9 to -6.8%.

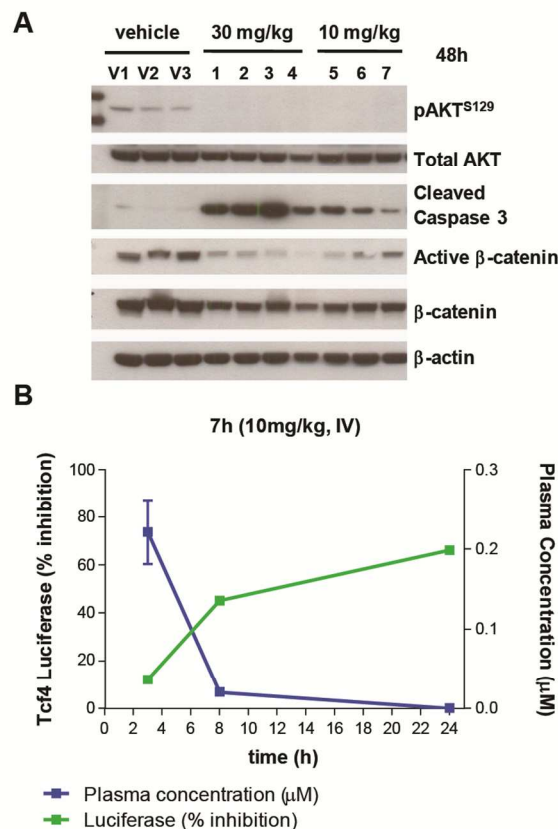


**Figure 6.** Inhibition of substrate (AKT<sup>S129</sup>) and downstream marker (active  $\beta$ -catenin) phosphorylation in SW620 xenografts by **7h** (10, 30 mg/kg, IV). Individual lanes correspond to vehicle or compound treated animals and are numbered. (A); Inhibition of Wnt/Tcf4 Topflash luciferase reporter activity in DLD-1 xenografts following treatment with **7h** (10 mg/kg, IV) (B).

In conclusion, we have identified a series of potent and selective CK2 kinase inhibitors that decrease AKT<sup>S129</sup> phosphorylation in cells and whose antiproliferative effects correlate with inhibition of Wnt luciferase reporter gene transcription. Using the *in vivo* probe **7h**, we have demonstrated a reduction in the downstream biomarkers pAKT<sup>S129</sup> and  $\beta$ -catenin and a high level of activity as a monotherapy in HCT-116 and SW-620 xenografts.<sup>18</sup> Further studies, using **7h** and related analogs, are planned to more fully understand the dependence of CRC on CK2-mediated Wnt pathway inhibition and will be reported in future communications.

#### SUPPORTING INFORMATION AVAILABLE:

Experimental details and characterization data for key compounds, crystallographic and biophysical protocols; active  $\beta$ -

catenin Western blot protocol. This material is available free of charge via the Internet at <http://pubs.acs.org>.

## CORRESPONDING AUTHOR:

\*(J.E.D.) E-mail: [james.dowling@astrazeneca.com](mailto:james.dowling@astrazeneca.com)

## ACKNOWLEDGMENTS:

The authors wish to thank Mei Su and Helen Xiaomei Feng for compound synthesis, Vicki Racicot and Zhong-Ying Liu for *in vitro* and *in vivo* biology support, respectively.

## ABBREVIATIONS USED:

heps: hepatocytes, CL: clearance, PK: pharmacokinetics, PD: pharmacodynamics, aq.: aqueous, sol.: solubility, PPB: plasma protein binding, CL<sub>int</sub>: intrinsic clearance, IP: intraperitoneal, IV: intravenous, Hu: human, ABT: aminobenzotriazole.

## REFERENCES:

- Niefind, K.; Guerra, B. Ermakowa, I.; Issinger, O.-G. Crystal structure of human protein kinase CK2: insights into basic properties of the CK2 holoenzyme. *Embo J.* **2001**, *20*, 5320-5331.
- Ruzzene, M.; Pinna, L. A. Addiction to protein kinase CK2: A common denominator of diverse cancer cells? *Biochim. Biophys. Acta* **2010**, *1804*, 499-504.
- Pierre, F.; Chua, P. C.; O'Brien, S. E.; Siddiqui-Jain, A.; Bourbon, P.; Haddach, M.; Michaux, J.; Nagasawa, J.; Schwaebe, M. K.; Stefan, E.; Vialettes, A.; Whitten, J. P.; Chen, T. K.; Darjania, L.; Stansfield, R.; Anderes, K.; Bliesath, J.; Drygin, D.; Ho, C.; Omori, M.; Proffitt, C.; Streiner, N.; Trent, K.; Rice, W.G.; Ryckman, D. M. Discovery and SAR of 5-(3-chlorophenylamino)benzo[c][2,6]naphthyridine-8-carboxylic acid (CX-4945), the first clinical stage inhibitor of protein kinase CK2 for the treatment of cancer. *J. Med. Chem.* **2011**, *54*, 635-54.
- Clevers, H.; Nusse, R. Wnt/ $\beta$ -Catenin Signaling and Disease, *Cell*, **2012**, *149*, 1192-1205
- Dominguez, I.; Sonenshein, G.E.; Seldin, D.C. CK2 and its role in Wnt and NF-kappa B signaling: Linking development and cancer. *Cell. Mol. Life. Sci.* **2009**, *66*, 1850-1857.
- Gao, Y.; Wang, H.-Y. Casein Kinase 2 Is Activated and Essential for Wnt/ $\beta$ -Catenin Signaling. *J. Biol. Chem.*, **2006**, *281*, 18394-18400.
- Tapia, J. C.; Torres, V. A.; Rodriguez, D. A.; Leyton, L.; Quest, A. F. G. Casein kinase 2 (CK2) increases survivin expression via enhanced  $\beta$ -catenin-T cell factor/lymphoid enhancer binding factor-dependent transcription. *PNAS*, **2006**, *41*, 15079-15084.
- Zou, J.; Luo, H.; Zeng, Q.; Dong, Z.; Wu, D.; Liu, L. Protein kinase CK2 $\alpha$  is overexpressed in colorectal cancer and modulates cell proliferation and invasion via regulating EMT-related genes. *Journal of Translational Medicine* **2011**, *9*, 97-108.
- Lin, K.-Y.; Tai, C.; Hsu, J.-C.; Li, C.-F.; Fang, C.-L.; Lai, H.-C.; Hseu, Y.-C.; Lin, Y.-F.; Uen, Y.-H. Overexpression of Nuclear Protein Kinase CK2  $\alpha$  Catalytic Subunit (CK2 $\alpha$ ) as a Poor Prognosticator in Human Colorectal Cancer. *PLoS One*, **2011**, *6*(2): e17193.
- Dowling, J. E.; Bao, L.; Brassil, P.; Chen, H.; Chuaqui, C.; Cooke, E. L.; Denz, C. R.; Larsen, N. A.; Lyne, P. D.; Peng, B.; Pontz, T. W.; Racicot, V.; Russell, D.; Su, N.; Thakur, K.; Wu, A.; Ye, Q.; Zhang, T. Potent and selective inhibitors of CK2 kinase identified through structure-guided hybridization. *ACS Med. Chem. Lett.* **2012**, *3*, 278-283.
- Johannes, J. W.; Almeida, L.; Barlaam, B.; Boriack-Sjodin, P. A.; Casella, R.; Croft, R. A.; Dishington, A. P.; Gingipalli, L.; Gu, C.; Hawkins, J. L.; Holmes, J. L.; Howard, T.; Huang, J.; Ioannidis, S.; Kazmirski, S.; Lamb, M. L.; McGuire, T. M.; Moore, J. E.; Ogg, D.; Patel, A.; Pike, K. G.; Pontz, T.; Robb, G. R.; Su, N.; Wang, H.; Wu, X.; Zhang, H. J.; Zhang, Y.; Zheng, X.; Wang, T. Pyrimidinone nicotinamide mimetics as selective tankyrase and Wnt pathway inhibitors suitable for *in vivo* pharmacology. *ACS Med. Chem. Lett.* **2015**, *6*, 254-259.
- PDB deposition codes for the co-crystal structures are: **5H8B (2)**, **5H8G (7b)**, **5H8E (7h)**.
- Figure produced using Pymol. DeLano, W. L. The PyMOL Molecular Graphics System; DeLano Scientific: San Carlos, CA, USA, 2002. <http://www.pymol.org>.
- See supplementary material.
- Karaman, M. W.; Herrgard, S.; Treiber, D. K.; Gallant, P.; Atteridge, C. E.; Campbell, B. T.; Chan, K. W.; Ciceri, P.; Davis, M. I.; Edeen, P. T.; Faraoni, R.; Floyd, M.; Hunt, J. P.; Lockhart, D. J.; Milanov, Z. V.; Morrison, M. J.; Pallares, G.; Patel, H. K.; Pritchard, S.; Wodicka, L. M.; Zarrinkar, P. P. A quantitative analysis of kinase inhibitor selectivity. *Nat. Biotechnol.* **2008**, *26*, 127-132.
- Di Maira, G.; Brustolon, F.; Pinna, L.A.; Ruzzene, M. Dephosphorylation and inactivation of Akt/PKB is counteracted by protein kinase CK2 in HEK 293T cells. *Cell. Mol. Life Sci.* **2009**, *66*, 3363-3373.
- Ponce, D. P.; Maturana, J. L.; Cabello, P.; Yefi, R.; Niechi, I.; Silva, E.; Armisen, R.; Galindo, M.; Antonelli, M.; Tapia, J. C. Phosphorylation of Akt/PKB by CK2 is necessary for the Akt-dependent up-regulation of  $\beta$ -catenin transcriptional activity. *J. Cell. Physiol.* **2011**, *226*: 1953-1959.
- Dowling, J. E.; Alimzhanov, M.; Bao, L.; Chuaqui, C.; Denz, C.; Ferguson, A.; Graff, C.; Liu, Z.-Y.; Lyne, P.; Racicot, V.; Wu, A.; Wu, J.; Ye, Q.; Cooke, E. L. Discovery and characterization of AZ968, a potent and selective inhibitor of CK2 kinase with effects on AKT signaling *in vivo*. Poster presented at the 103rd Annual Meeting of the American Association for Cancer Research, March 31-April 4, 2012. Chicago, IL. Abstract No. 3907.

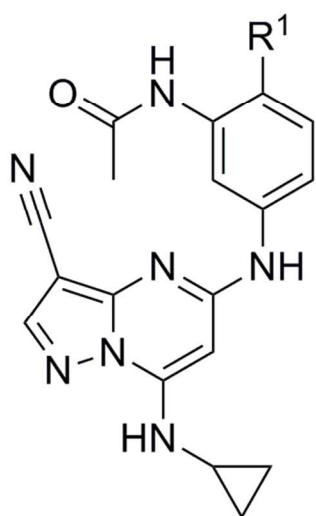
**1 (R<sup>1</sup> = H)**CK2 IC<sub>50</sub> = 9 nMpAKT IC<sub>50</sub> = 0.066 μMWnt DLD-1 reporter IC<sub>50</sub> = 0.84 μM**2 (R<sup>1</sup> = Me)**CK2 IC<sub>50</sub> < 3 nMpAKT IC<sub>50</sub> = 0.002 μMWnt DLD-1 reporter IC<sub>50</sub> = 0.06 μM

Figure 1. Early pyrazolo[1,5-a]pyrimidine leads (1 & 2).  
88x46mm (300 x 300 DPI)

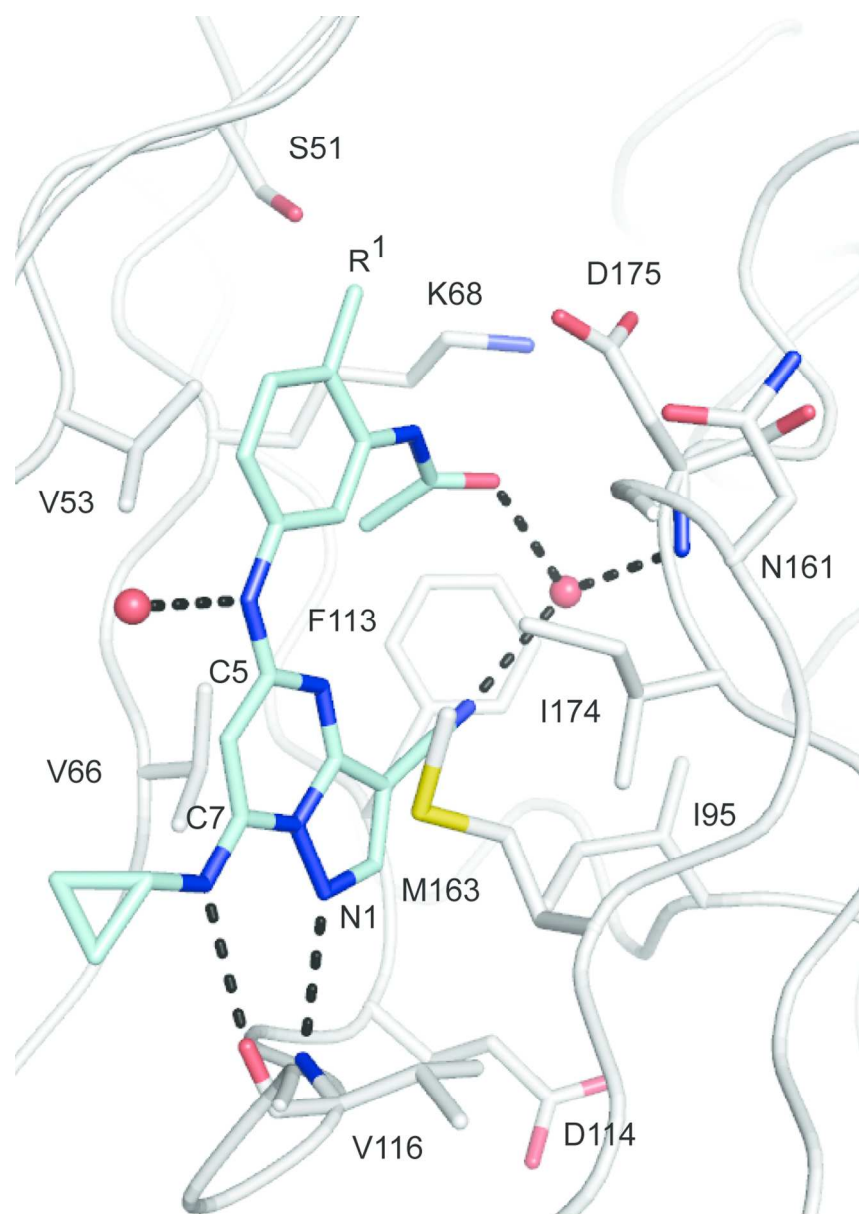
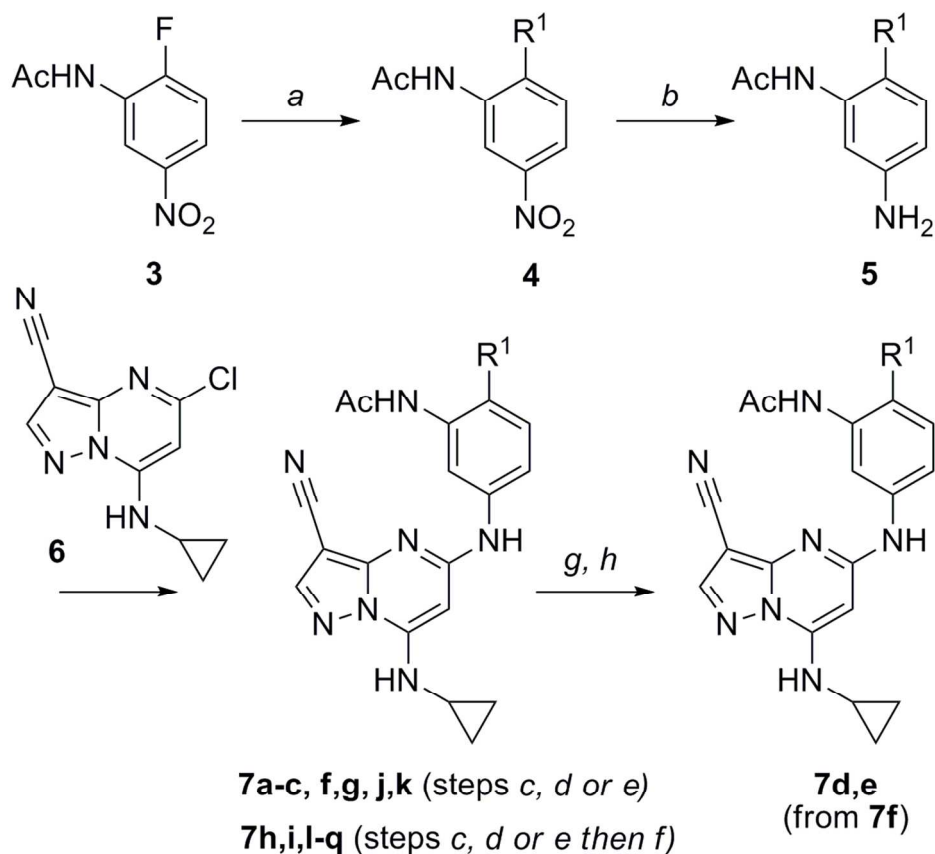


Figure 2. X-ray crystallographic structure of human CK2 $\alpha$  in complex with compound 2 determined at 2.55 Å resolution (PDB accession code: 5H8B).<sup>12, 13</sup> Water molecules are shown as red spheres. Hydrogen bonds to the inhibitor are shown as black dashed lines.<sup>14</sup>  
104x146mm (300 x 300 DPI)



35 <sup>a</sup>Reagents and conditions: (a) R,R'NH, Cs<sub>2</sub>CO<sub>3</sub>, DMF, 80 °C; (b) H<sub>2</sub>, Pd/C,  
 36 MeOH, 25 °C; (c) **6**, 5 mol% Xantphos, 10 mol% Pd<sub>2</sub>(dba)<sub>3</sub>, Cs<sub>2</sub>CO<sub>3</sub>, DMA,  
 37 150 °C in a microwave; (d) **6**, KF, NMP or DMSO, 150 °C; (e) **6**, 20 mol%  
 38 tBuXphos, 10 mol% Pd<sub>2</sub>(dba)<sub>3</sub>, Cs<sub>2</sub>CO<sub>3</sub>, NMP/Dioxane, 100 °C; (f) TFA,  
 39 CH<sub>2</sub>Cl<sub>2</sub>, 25 °C; (g) **7f**, pyridine, MsCl, 0 °C; (h) R,R'NH, MeCN, 65 °C.

40  
41  
42  
43 Synthesis of compounds 7a-q.  
 44 108x118mm (300 x 300 DPI)

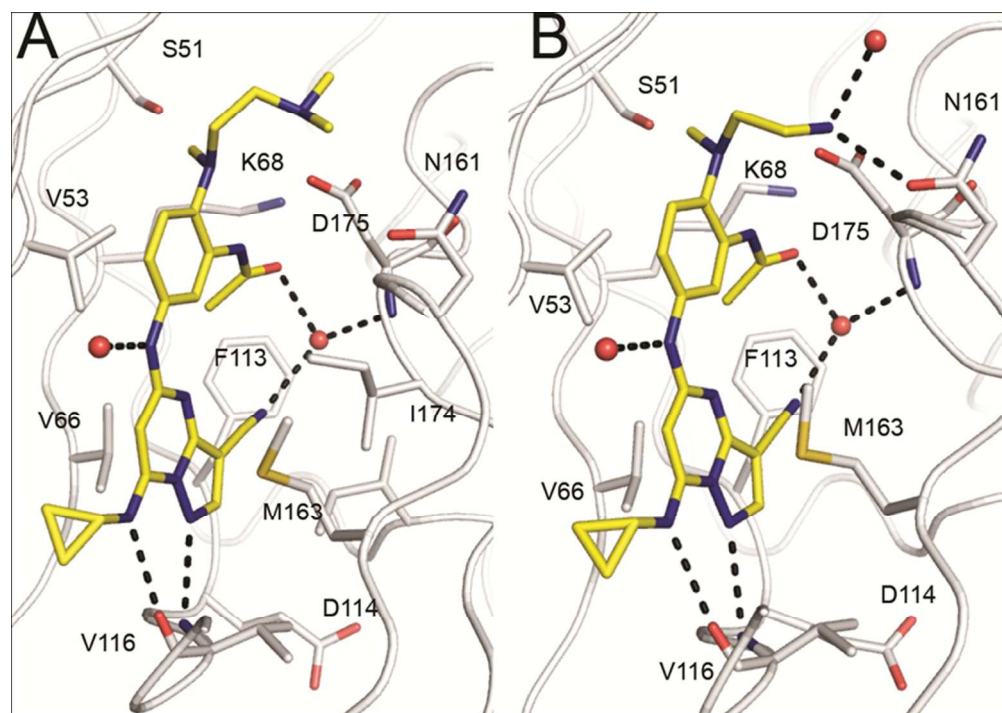


Figure 3. X-ray crystallographic structure of human CK2 $\alpha$  in complex with compounds 7b (A) and 7h (B) determined at 2.00 Å and 2.15 Å resolution (PDB accession codes: 2TBD and 3TBD).<sup>12,13</sup> Water molecules are shown as red spheres and hydro-gen bonds to the inhibitor are shown as black dashed lines.<sup>14</sup>

152x107mm (150 x 150 DPI)

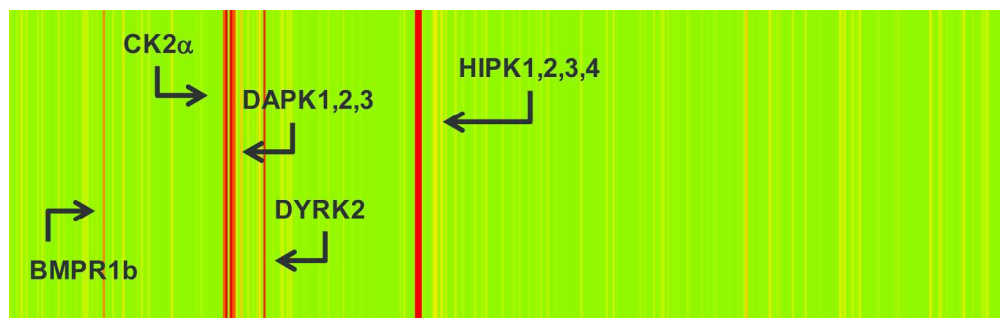


Figure 4. Kinase selectivity profile for 7h when tested at a concentration of 0.1  $\mu\text{M}$  against a panel of 402 kinases.  
216x67mm (300 x 300 DPI)

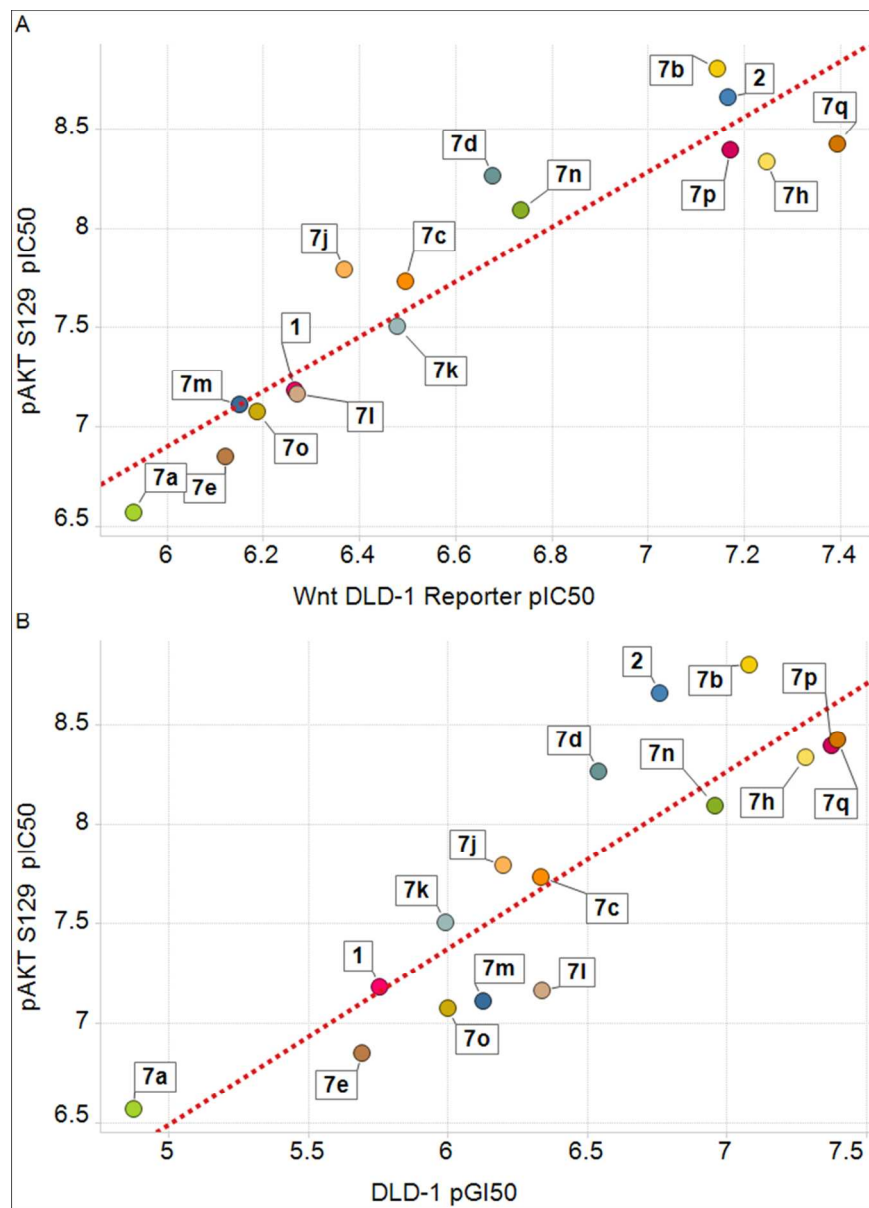


Figure 5. Relationship between pAKTS129 depletion and Wnt Topflash reporter inhibition in DLD-1 cells (A). Relationship between pAKTS129 depletion and growth inhibition in DLD-1 cells (B). 194x269mm (150 x 150 DPI)

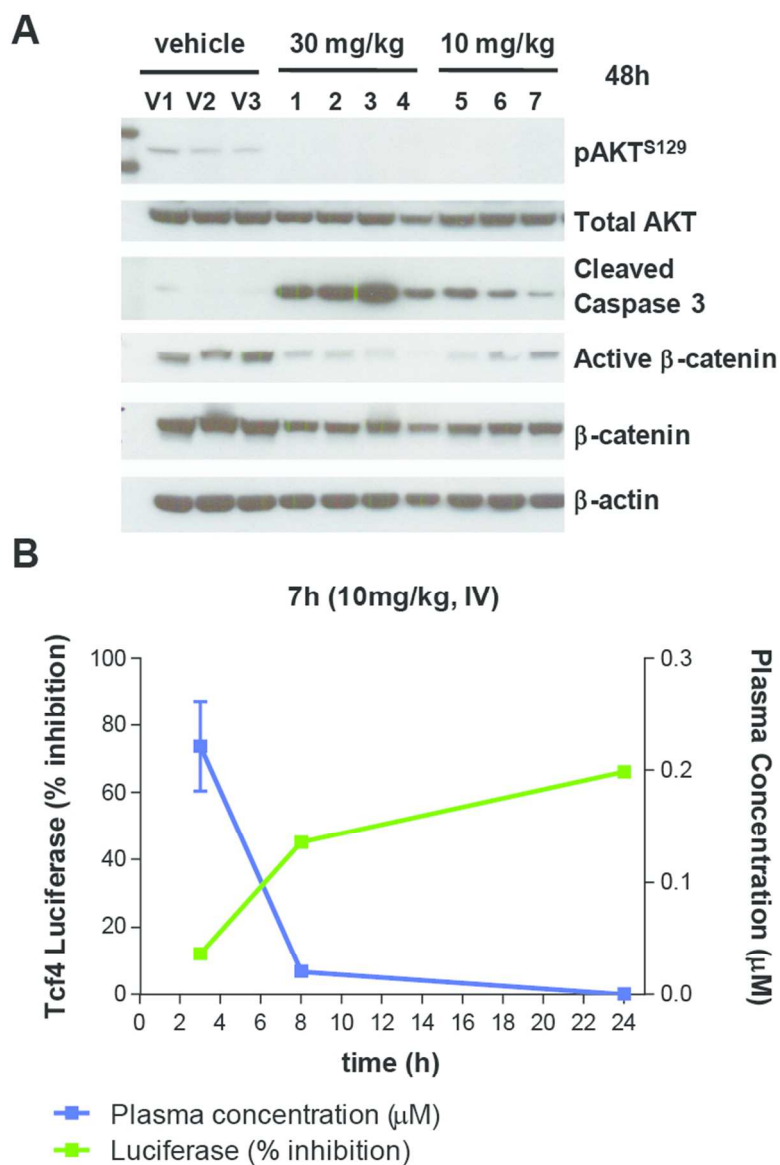
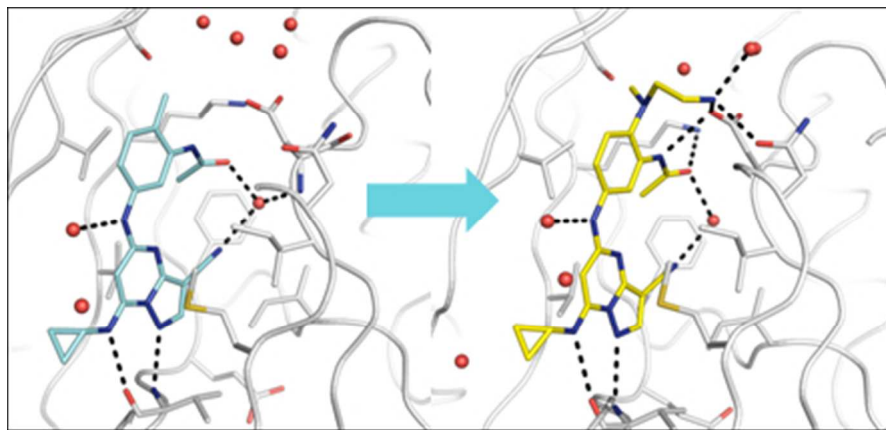


Figure 6. Inhibition of substrate (AKTS129) and downstream marker (active  $\beta$ -catenin) phosphorylation in SW620 xenografts by 7h (10, 30 mg/kg, IV). Individual lanes correspond to vehicle or compound treated animals and are numbered. (A); Inhibition of Wnt/Tcf4 Topflash luciferase reporter activity in DLD-1 xenografts following treatment with 7h (10 mg/kg, IV) (B).  
145x205mm (150 x 150 DPI)



75x35mm (150 x 150 DPI)